

Inferring Average Ground Profiles of the Muon Density of Inclined Air Showers from Monte-Carlo Simulations at Ultra-High Energy

Hans Dembinski ^{a,*}, Pierre Billoir ^b, Olivier Deligny ^c, and Thomas Hebbeker ^a

^a*III. Physikalisches Institut A, RWTH Aachen University, Germany*

^b*LPNHE (Universités Paris 6 & 7, CNRS-IN2P3), Paris, France*

^c*IPN, CNRS/IN2P3-Université Paris Sud, Orsay, France*

Abstract

A standard method to measure ultra-high energy cosmic rays is the sampling of the ground particle profile of the extensive air shower that is produced in the atmosphere with an array of surface detectors.

The primary energy of inclined air showers with zenith angles $> 60^\circ$ can be reconstructed by using simulated 2-D profiles of the ground density of muons. We will present an effective way to extract such profiles from a library of Monte-Carlo simulated air showers. Also, we will demonstrate a way to speed up the simulation of ground profiles of the muon density in very inclined showers by three orders of magnitude, if only the muon component in the shower is of interest.

Key words: UHECR, inclined air shower, simulation, energy reconstruction, ground profile, Pierre Auger Observatory

1 Introduction

Ultra-high energy cosmic rays (UHECRs) have triggered interest for several decades. Many experimental efforts to measure their arrival directions, their nature and their energy spectrum have been made.

* Corresponding author.

Email address: dembinski@physik.rwth-aachen.de (Hans Dembinski).

Even if their origin remains unknown, recent measurements of the Pierre Auger Observatory show that at ultra high energies, the arrival directions of UHE-CRs correlate with the distribution of nearby Active Galactic Nuclei [20], which opens the window to cosmic ray astronomy. These observations certainly constitute a major step forward in understanding the origin of UHECRs.

All these measurements need a large experimental exposure to gain the necessary statistic despite the low flux of roughly 1 particle per km^2 and per year above $E = 10^{19}$ eV. Extensive surface arrays of particle detectors are the successful solution to gather these statistics. They observe extensive air showers on the ground, which are generated by UHECRs in our atmosphere.

For the standard case of primary nuclei, air showers consist mainly of photons, electrons, and muons. In this note, we will focus on the special case of very inclined showers with zenith angles $\theta > 60^\circ$ and energies $E > 10^{18}$ eV. Our main interest will be the muon component of the shower.

At these inclinations, the penetrating muons start to dominate the shower profile on the ground, while the electromagnetic shower component gets almost completely absorbed in the atmospheric matter (see Fig. B.1 in the appendix). The muons form a nearly flat disc with a radius of several kilometers that hits the ground with the speed of light. The shower direction can be reconstructed by measuring the different arrival times of the disc at several positions in the array of surface detectors.

For the energy reconstruction, we can exploit special properties of the spatial profile of the muon density n_μ , which we get by integrating the muon flux through the ground plane over the time of a single shower event. This profile is in general a function of the properties of the primary cosmic ray and the observation site:

$$n_\mu = n_\mu(x_g, y_g; \theta, \phi, E, A; \mathbf{B}, h_g, \rho_{\text{air}}(h)), \quad (1)$$

where (x_g, y_g) are ground coordinates relative to the shower core, which we define as the point where the shower axis pierces the ground plane. θ is the zenith angle, ϕ the azimuth angle, E the energy, and A the atomic number of the primary nucleus; whereas \mathbf{B} is the geomagnetic field, h_g the altitude of the ground level, and $\rho_{\text{air}}(h)$ the air density profile at the observation site. We will now simplify this relation.

In a first step, we turn the last three variables into constants by selecting a specific observation site – we use the Southern Pierre Auger Observatory in Malargüe, Argentina¹. We will omit these variables in the rest of the paper.

¹ The atmospheric profile $\rho_{\text{air}}(h)$ and the geomagnetic field \mathbf{B} vary weakly with time. The influence of the former on shower observables is discussed in [15], the latter

In Section 2 we will summarise general features of very inclined air showers, that have been discussed before [1, 2, 5]. An important property will be that n_μ can be factorised in good approximation into the total muon number N_μ on the ground, which is function of E and A and θ , and a normalised spatial profile p_μ , which is only a function of the shower direction (see also [1, 2]):

$$n_\mu(x_g, y_g, \theta, \phi, E, A) \simeq p_\mu(x_g, y_g, \theta, \phi) \times N_\mu(\theta, E, A) \text{ for } \theta > 60^\circ, \quad (2)$$

We will see, that N_μ is practically independent of ϕ , the remaining θ dependency is a result of the varying influence of muon decay, as more inclined showers travel longer paths through the atmosphere.

If we consider a fixed zenith angle θ and atomic number A , the relation between muon ground number N_μ and energy E is mainly given by energy conservation. Shower cascade physics show, that the relation is actually a power law [9, 17]:

$$N_\mu(\theta, E, A) \propto E^\beta, \quad (3)$$

where $\beta \lesssim 1$ is a constant in good approximation between $E = 10^{18}$ eV and 10^{20} eV. More details are given in Section 2.

If an air shower reaches the ground, a surface array of particle detectors samples the time integrated muon flux and thus the muon density profile n_μ at several points on the ground. With the independently measured shower direction (θ, ϕ) from the muon arrival times and a normalised profile $p_\mu(x_g, y_g, \theta, \phi)$ extracted from simulations, the shower energy E can be reconstructed by fitting $n_\mu = N_\mu \times p_\mu$ to the sampled muon densities, with the intersection point between shower axis and ground and N_μ as free parameters. The primary energy E can then be calculated from N_μ through a calibration function, that is either derived from simulations or from experimental measurements.

A good knowledge of the normalised muon density profile $p_\mu(x_g, y_g, \theta, \phi)$ from simulations is necessary for this approach. A purely analytical description of p_μ is difficult, but a semi-analytical model exists, which relies in parts on air shower simulations [1]. This semi-analytical model was already applied successfully in air shower experiments [2]. The semi-analytical approach offers much insight into the physical processes, which shape the normalised profile of the muon density, but it also introduces some approximations with respect to a full Monte-Carlo simulation.

In this paper, we want to follow a different paradigm to obtain p_μ . In Section 4, we establish a very general parameterisation function which can be fitted to the Monte-Carlo simulations directly. The parameterisation function is a

varies by about 1° in direction and 2% in magnitude over 10 years in Malargüe [18].

linear combination of basic functions, which allows to fit a large number of free parameters in an efficient way. The parameters do not necessarily contain much physical meaning, but they make the parameterisation flexible enough to follow most details of the raw Monte-Carlo simulation. A final comparison of the parameterisation of $p_\mu(x_g, y_g, \theta, \phi)$ with raw Monte-Carlo showers shows the power of this approach.

The whole procedure to obtain the fitted parameterisation was optimised so that it can be applied to nearly any existing Monte-Carlo library of very inclined showers. The library which was used in this work is described in Section 3. We will further present an efficient way to speed up the simulation of muon ground profiles of inclined showers, which can be used as an input for our parameterisation method. To get the increase in speed, we will exploit an azimuthal symmetry of the muon distribution at their production point and neglect the calculation of the electromagnetic cascade.

The energy E of very inclined showers cannot be reconstructed with the established standard methods for showers with $\theta < 60^\circ$ (see Section 2), therefore inclined showers are often discarded. On the other hand, they make up 25 % of all events in an ideal surface array of particle detectors. Recovering these showers yields a gain in event statistics of the same order. The ability to reconstruct inclined showers also increases the field of view of the detector, and thus the total observable region of the sky at the site of the experiment. This is in particular relevant for anisotropy searches. Because the primary electromagnetic shower is absorbed in the atmosphere, very inclined showers also give an opportunity to study the muon component of a shower, even with a surface detector array that cannot distinguish well between photons, electrons and muons.

2 Inclined air showers: the general picture

2.1 *The ground particle profile*

To discuss the ground profile of muon density n_μ , it is useful to introduce a special coordinate system: the traditional shower front plane coordinate system (see Fig. 1). The shower front plane is perpendicular to the shower axis and orientated so that the projected magnetic field is parallel to the y -axis. The origin of this coordinate system is the point where the shower axis pierces the ground plane.

All observations are still done in the ground plane, but projected onto this plane. It has the advantage, that it preserves some of the principal symmetries

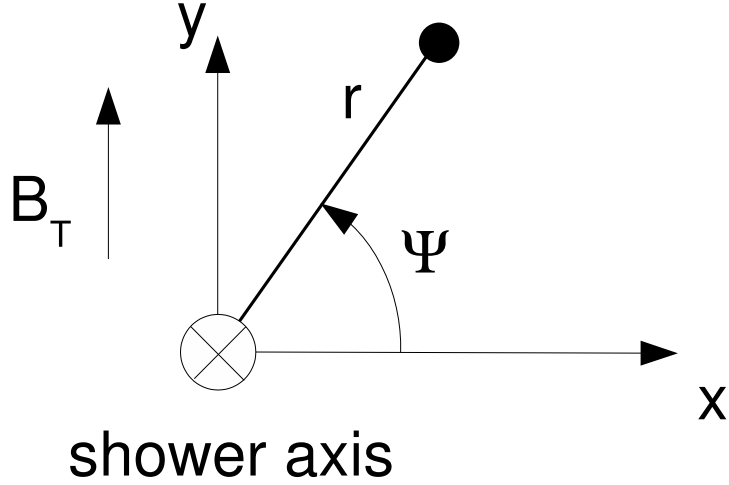


Fig. 1. Shower front plane coordinate system, adopted from [1]. e_z is anti-parallel to the momentum vector of the shower, e_y is parallel to \mathbf{B}_T , the component of the geomagnetic field perpendicular to the shower axis. ψ and r are polar coordinates in this lateral plane.

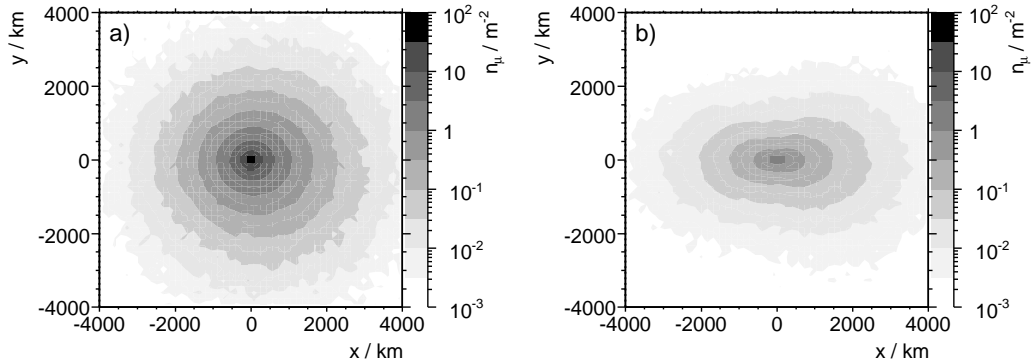


Fig. 2. Simulated ground profile of the muon density n_μ at $E \approx 10^{19}$ eV and $\phi \approx 0^\circ$, projected into the shower front plane. The two plots illustrate the radial symmetry loss at large inclinations. a) At $\theta \approx 60^\circ$, the radial symmetry around the shower axis is still dominant. b) At $\theta \approx 80^\circ$, geomagnetic deflections break this symmetry by separating muons of opposite charge (see text). The azimuthal angle ϕ is chosen such, that the geomagnetic deflections are at their maximum. Both showers are taken from the library described in Section 3.2.

of the shower profile. We will refer to this coordinate system during the rest of the paper.

We use the convention of the Pierre Auger Observatory for the azimuthal angle ϕ , where a shower arriving from the geographic East equals to $\phi = 0^\circ$, and a shower from the geographic North equals to $\phi = 90^\circ$.

The ground profile of muon density n_μ has different properties for standard

showers ($0^\circ < \theta < 60^\circ$) and for very inclined showers ($60^\circ < \theta < 90^\circ$). Standard showers are photon and electron rich at ground level, and the flux of particles through the shower front plane is almost radially symmetric with respect to the shower axis, and thus independent of ψ and ϕ .

On the contrary, very inclined showers travel on much longer paths through the atmosphere. This results in an absorption of the electromagnetic component and in a deformation of the surviving muon component by the geomagnetic field.

The ground profile of very inclined showers is therefore muon rich, and the flux of particles through the shower front plane is not independent of ψ . Since the magnetic deformation of the shower depends on the orientation of the shower axis to the fixed geomagnetic field, there is also a dependency on azimuth ϕ .

In addition, muons in the early arriving part of the shower travel shorter distances and with a different inclination than muons in the late arriving part of the shower. This leads to additional asymmetries which need to be taken into account.

The loss of radial symmetry in the shower front plane due to the geomagnetic deformation at large inclinations is illustrated in Fig. 2.

2.2 *The muon component of hadronic showers*

An air shower induced by a proton or a nucleus first produces a hadronic cascade, leading after some steps to charged and neutral pions. These pions feed an electromagnetic component through the decay of π^0 's, and a muon component through the decay of π^+ and π^- . As the zenith angle rises from $\theta = 0^\circ$ to 90° , the total atmospheric depth X_{atm} of the atmosphere increases from 900 g cm^{-2} to 31000 g cm^{-2} for an observer at the Auger Southern site (see Fig. 3).

Above $\theta = 60^\circ$, the total atmospheric depth X_{atm} is much larger than the depth of the air shower maximum $X_{\text{max}} \approx 750 \text{ g cm}^{-2}$ [22], where most particles are produced and the hadronic cascade dies out (see also Fig. B.1 in the appendix).

Muons are produced at the end of the hadronic cascade, when the energy of the charged mesons is diminished so much that their decay length $\beta\gamma c\tau$ becomes smaller than their interaction length, which is proportional to the inverse of the air density. At large zenith angles, the hadronic cascade develops almost entirely in the upper atmosphere, where the hadronic interaction length is a few kilometers. The Lorentz factor γ of decaying mesons is then of the order of 1000 for cosmic rays around 10^{18} eV, which leads to typical muon energies of

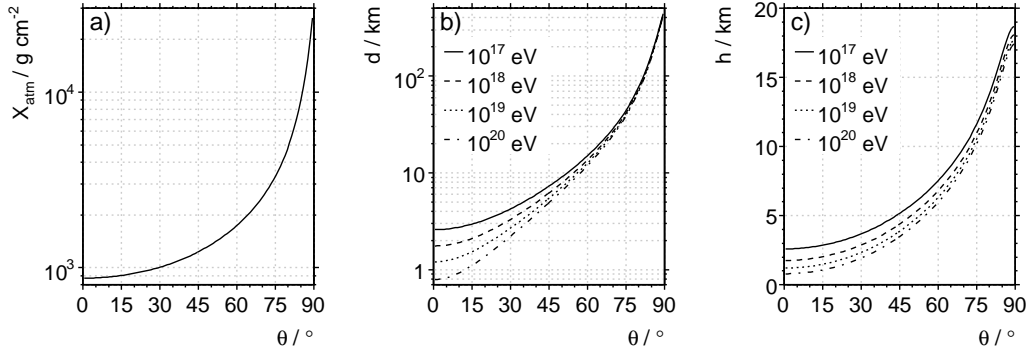


Fig. 3. For an observer at the Auger South altitude of 1400 m we calculated: a) the total integrated atmospheric depth along the shower path X_{atm} , b) the distance d between the shower maximum and the core on the surface along the shower axis, and c) the altitude of the shower maximum above ground h as a function of zenith angle θ . The calculation uses a parameterisation of the atmospheric depth of the U.S. standard atmosphere in [15] and a parameterisation of the depth of the electromagnetic shower maximum as a function of the shower energy $X_{\text{max}}(E)$ as measured by the Pierre Auger Observatory [22]. Since the depth of the electromagnetic shower maximum only approximates the point of the muon production, the values of d and h are also only approximate.

100 GeV and small angular divergences from the shower axis $\lesssim 1/\gamma$. Practically all muons in the shower are ultra-relativistic.

After their production, muons are affected by ionisation and radiative energy losses, multiple scattering, decay, and geomagnetic deflections.

The energy losses are moderate, about $2 \text{ MeV cm}^2 \text{ g}^{-1}$ [25], which translates to about 2 GeV (60 GeV) for a shower at $\theta = 60^\circ$ (90°). Decays are only relevant for low energy muons. The decay length of a typical 100 GeV muon is 620 km and thus much larger than the distance d from the production point to the ground for all but the largest zenith angles (see Fig. 3).

Geomagnetic deflections δx for muons in air showers can be approximated as [1]:

$$\delta x \simeq \frac{e B_T d^2}{2E_\mu/c}, \quad (4)$$

where e is the elementary charge, d the distance between the muon production point and the ground along the shower axis, E_μ is the muon energy, and B_T is the perpendicular component of the geomagnetic field with respect to the muon direction. The amount of geomagnetic deflection therefore implicitly depends on azimuth angle ϕ of the shower. In the extreme case, a muon propagates in a $26 \mu\text{T}$ geomagnetic field at the Auger South site. For a 50 GeV muon at a zenith angle of $\theta = 60^\circ$ (80°), this leads to about 10 m (400 m) lateral displacement after 13 km (70 km) travelled distance to the Auger South ground level. For practically all muons, the increased path length through the

geomagnetic deflection δx is negligible compared to the muon decay length. It follows, that the total muon number N_μ on the ground does not depend on the azimuth angle ϕ .

We can summarise, that the muonic component of inclined air showers remains active and quite collimated down to the ground whatever the zenith angle θ .

The primary electromagnetic component coming from π^0 decay is already quite absorbed in the atmosphere when the shower reaches the ground at $\theta = 60^\circ$, and can be considered extinct above $\theta = 70^\circ$ (see also Fig. B.1).

A non-negligible electromagnetic component is still detectable on the ground at all angles, which is produced by the muons themselves. The muons produce photons and electrons through decay, bremsstrahlung, pair production and delta rays along their path through the atmosphere. In some sense, they are surrounded by electromagnetic sub-showers with a moderate lateral extension – typically a few tens of meters. These electromagnetic particles arrive together with the muons within a few tens of nanoseconds [6], and in such a way, that they do not increase the thickness of the shower front.

Moreover, if the density of muons is larger than 0.1 m^{-2} , which is the case in a large part of the shower footprint on the ground for the primary energies above 10^{18} eV (see Fig. 2), these electromagnetic sub-showers largely overlap, and they result in a continuous halo that has to be considered in particle detectors that cannot distinguish between muons and the electromagnetic halo.

2.3 Energy scaling and universality of the density profile of muons

It was discussed in the previous section, that the energy and angular divergence distributions of muons at their production point are a function of the air density $\rho_{\text{air}}(h)$ in the altitude h . On the ground level, the muon energy loss, the fraction of muons that decay, and the geomagnetic deflection also depend on the distance d between the production point and the ground.

For inclined showers with $\theta > 60^\circ$, both h and d vary only little with energy (see Fig. 3). We therefore expect, that the muon density profile n_μ can be factorised into an energy independent normalised profile p_μ , and a global factor, which is the total muon number on the ground N_μ (see Eq. (2)).

This essential feature was already discussed in [2] based on simulations with the air shower code AIRES [21] and the hadronic interaction model [8]. Since it is such a central property, we checked it again with our library based on a different simulation code and model (see Fig. 4). For proton showers with $\theta > 60^\circ$, the normalised ground profile of the muon number p_μ varies within

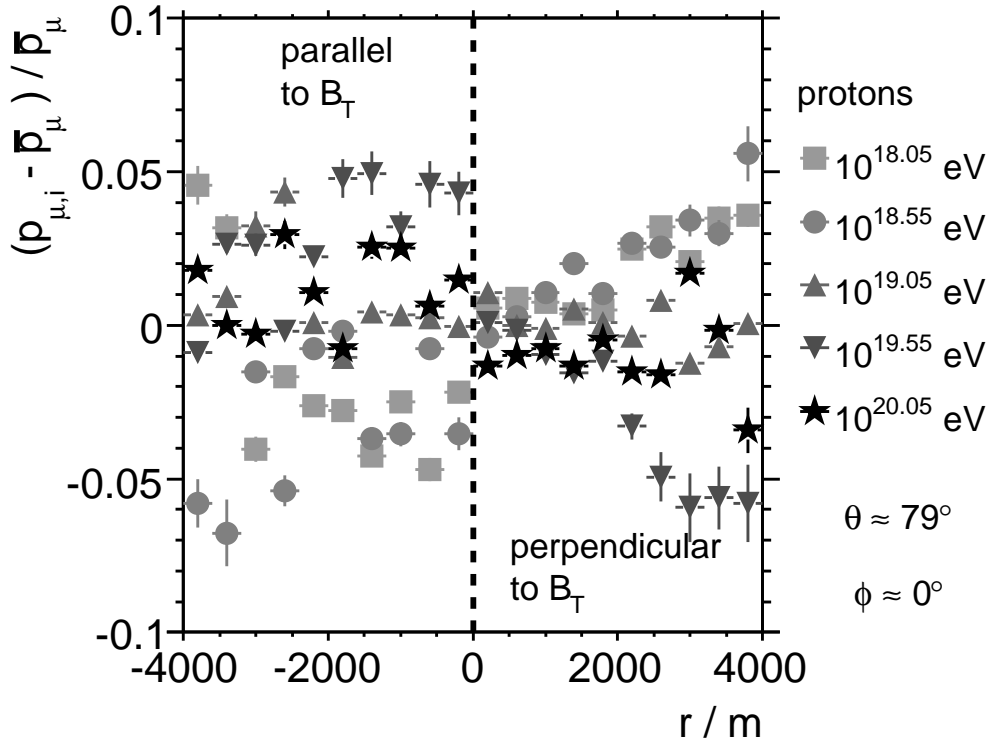


Fig. 4. Relative deviation from the average density profile of muons at ground as a function of primary energy for proton showers. The left (right) hand curve shows the density profile parallel (perpendicular) to the magnetic field projected into the shower plane \mathbf{B}_T . The error bars indicate the size of the intrinsic shower-to-shower variations of the density profile. For each curve, 10 proton showers from the library described in Section 3.2 were normalised at $r = 1000$ m and averaged.

5 % between 10^{18} eV and 10^{20} eV, with shower-to-shower fluctuations smaller than 1 %.

The normalised profile p_μ is also stable against variations of the atomic number A of the primary nuclei, as already discussed in [3, 4]. If we compare the two extreme cases of proton and iron primaries in simulations at $\theta > 60^\circ$, the normalised profile of the muon density p_μ again varies within 5 % (see Fig. 5).

The same applies for other detector-relevant muon ground observables, like the ground profile of muon energy $E_\mu(x, y)$ and the ground profile of muon inclination $\theta_\mu(x, y)$.

The variation of p_μ is thus much smaller than the typical shower-to-shower fluctuations of the total muon number at ground N_μ for primary protons, which are on the level of 13 % in our simulation. The fluctuations of N_μ are a natural limit to the obtainable energy resolution from a muon detector array. The variation of the normalised profile p_μ is negligible in comparison.

The total number of muons N_μ on the ground depends on the zenith angle

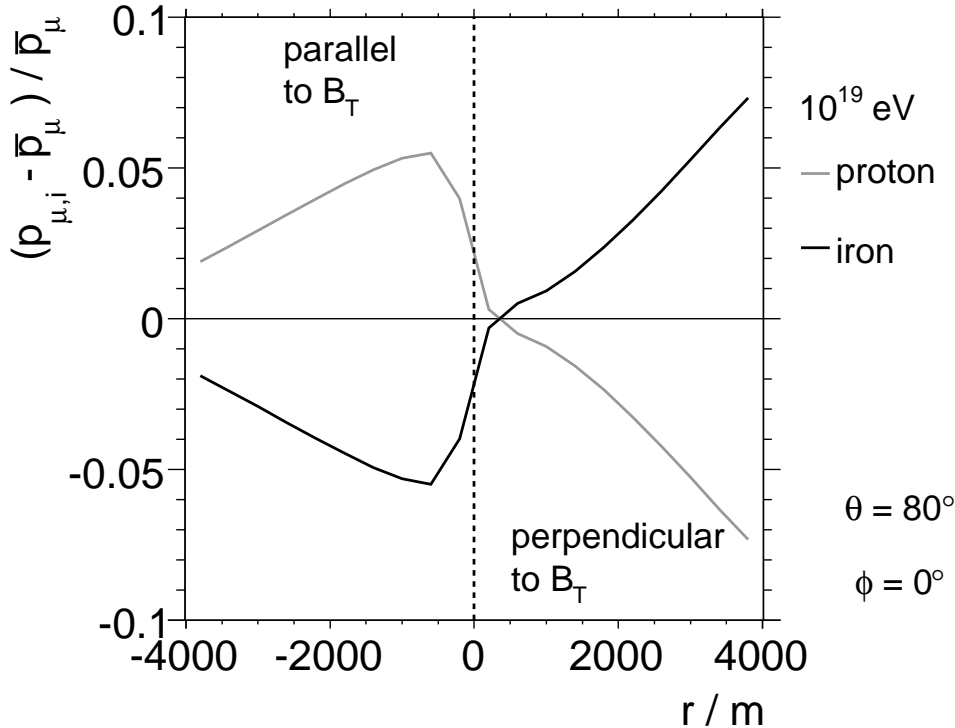


Fig. 5. Relative deviation from the average density profiles of muons at ground for proton and iron primaries. The proton and the iron profile were generated by averaging 50 showers of 10^{19} eV, generated with the air shower code AIRES [21] and the hadronic interaction model QGSJet01 [14]. Both profiles were normalised at $r = 1000$ m.

θ , on the primary energy E , and on the atomic number A of the primary nucleus. Because the air shower is so well beyond its shower maximum, the zenith angle and energy dependence factorise. This holds for proton and iron primaries alike, as the difference in the depth of the shower maximum is only about 100 g cm^{-2} [22]. The energy dependence can be calculated from cascade equations and turns out to be a power law:

$$N_{\mu} \simeq C_1(\theta) \times C_2(A) \times E^{\beta} \text{ for } \theta > 60^\circ, \quad (5)$$

where $\beta \lesssim 1$ is in principle a function of energy and atomic number. Fortunately, the energy dependence of β is weak, and can be neglected between $E = 10^{18}$ eV and 10^{20} eV for fixed type of primary nucleus [9, 17].

Let us point out that the total number of muons $N_{\mu}(\theta, E, A)$ is very sensitive to the theoretical modelling of the first interactions at ultra high energies. The disagreement between different models is of the same order as the difference between iron and proton showers, about 40 % – 50 % [2, 24]. The normalised profile p_{μ} varies with different air shower simulations to a much lesser degree, because the energies at which most muons are produced are within the reach of accelerator experiments and the muon interactions in the atmosphere are

Table 1

Parameter distribution of the proton shower library generated with CORSIKA/QGSJet-II/FLUKA [7, 10, 19]. $\delta_B = -4.2^\circ$ is the magnetic declination in Malargüe. The showers in the library are distributed in small finite regions of the parameter space. The distribution within each region is given in the table. Each region contains five showers and there are 1800 showers in total.

Parameter	distribution	low edge of region	width of region
$\lg E/\text{eV}$	flat	18.0, 18.5, 19.0, 19.5, 20.0	0.1
$\theta/^\circ$	$\sin(\theta) \cos(\theta)$	60, 70, 74, 78, 82, 86	2
$(\phi + \delta_B)/^\circ$	flat	0, 30, 60, 90, 120, 150, 180, 210, 240, 270, 300, 330	10

well understood.

3 Monte-Carlo simulation of muon ground profiles

A prerequisite for the extraction of the average ground profile is a library of simulated showers. This section will discuss the full simulation used in this note, and an alternative fast simulation that is able to speed up the generation of muon ground density profiles. We demonstrate the validity of the fast approach in a comparison of the muon ground profiles in Section 4.

3.1 Hadronic interactions and air shower thinning

The modeling of hadronic particle production in extensive air showers is subject to considerable theoretical uncertainties. On the one hand, most hadronic interactions are "soft" processes with small momentum transfer and cannot be calculated within perturbative QCD. On the other hand, the center of mass energy in the collision of a 10^{20} eV proton with a nitrogen nucleus is about 400 TeV, which is far beyond the experimental reach of current laboratory experiments.

Therefore one has to rely on phenomenological models that describe soft interactions by an effective theory. Hadronic interactions are split into multiple scattering processes that take place simultaneously, and each individual scattering process is modeled by a Pomeron exchange. A Pomeron exchange is equivalent to a microscopic quark-gluon cascade ("QCD parton ladder"), which mediate the interaction between the participating hadrons [19].

Another important issue in air shower simulations is the large number of secondary particles. A primary proton of 10^{20} eV produces about 10^{11} secondary

particles, most of them are low energy electromagnetic particles. To calculate such a shower in reasonable time, a *thinning* method has to be applied [11].

Modern forms of thinning are usually implemented such, that the first and final stages of the shower development are calculated in detail. In the intermediate thinning phase, basically all products of a particle interaction are deleted from the simulation except a survivor i , which is picked at random with a probability p_i proportional to its energy E_i . The survivor then gets a weight w_i , which conserves the total energy of the shower:

$$p_i = E_i / \sum_j E_j \quad w_i = 1/p_i, \quad (6)$$

where $\sum_j E_j$ is the energy sum over all products [10].

The thinning procedure introduces artificial fluctuations in physical observables of the shower. The thinning phase is usually made as short as possible, to keep the artificial fluctuations small against the natural fluctuations that appear during the shower development.

3.2 Full simulation chain

The maps presented in this note are extracted from a general purpose library of 1800 proton showers, which were generated with the CORSIKA [10] shower Monte-Carlo code. For the high and low energy interactions, the QGSJet-II [19] and FLUKA [7] models were used, respectively.

We made a choice to distribute the showers in small finite bins in the three-dimensional parameter space of energy, zenith and azimuth angle. This leaves gaps, where no showers were simulated, while other parts get a higher statistical coverage. The distribution of the showers inside the library is summarised in Table 1.

Technical details on the simulation options, the used thinning parameters and low energy cut-offs can be found in Appendix A.

The ground plane altitude h_g and the geomagnetic field \mathbf{B} are adapted to the Pierre Auger site in Malargüe, Argentina:

$$B = 24.6 \mu\text{T} \quad \delta_B = 4.2^\circ \quad \theta_B = -35.2^\circ \\ h_g = 1425 \text{ m},$$

with δ_B and θ_B as the geomagnetic declination and inclination.

The calculation of one shower takes roughly 1 day on a Pentium Xeon 2.8 GHz

CPU.

3.3 Fast simulation chain

As already emphasized, the ground profile of inclined showers depends on azimuth ϕ , which requires to run the full detailed simulation for each azimuth. Also, each full simulation spends a lot of CPU time on the calculation of the electromagnetic cascade.

If only muon profiles are to be extracted from the library, the simulation of the electromagnetic cascade is not needed, and the simulation can be sped up by a huge factor.

In this section, we describe an efficient procedure implementing the production of the muon profiles at ground without spending time to simulate the electromagnetic cascade.

We exploit, that the development of the hadronic cascade is almost independent of the magnetic field, and the magnetic deflections before the muon production can be neglected. This implies that the energy, direction and position of a muon at its production point is independent of the azimuth. Thus we need to simulate the muon distribution at their production point only once, and then generate ground distributions out of these initial muons for many azimuthal angles ϕ . Our procedure follows three steps.

A) Simulation of muons at their production point. For a given energy and zenith angle, a single value of ϕ is simulated (in practice along the magnetic north direction). High energy thresholds make sure, that no time is lost in following the details of the electromagnetic cascade (the numbers are given in Appendix B).

We then record² the position, energy, direction and statistical weight of the muons at their production point, provided their probability to reach the ground is not negligible.

B) Unthinning of the muon distribution. Muons at their production point may carry a weight from the thinning discussed in Section 3.1. To reduce artificial fluctuations of the muon profile on the ground, the thinning is reversed.

² This needs a modification of the shower Monte-Carlo code.

We take benefit of the cylindrical symmetry of the shower at the production point: A muon of weight ω is transformed into a set of n clones, with:

$$n = \omega/\omega_0 \quad \text{and} \quad \omega_1 = \omega/n \quad (7)$$

where ω_1 is the residual weight of each clone, and ω_0 is chosen between 5 and 50, depending on the primary energy E . The clones are identical, except for a random rotation of the position and the direction around the shower axis.

Typically, a few million muons per shower are regenerated. Compared to the full simulation, their weights w_1 are about 100 times smaller, which greatly reduces the density fluctuations at ground level.

C) Dedicated muon Monte-Carlo simulation. The recorded unthinned muons are then propagated to the ground level h_g for several values of the azimuth angle ϕ by a dedicated muon propagation code. The muon path is tracked in finite steps of 1 km (less at low energies). When the muons hit the ground, the last simulation step is adjusted to match exactly the nominal altitude h_g .

After a global rotation of their directions with respect to the new azimuth ϕ , the tracks are bent individually in the magnetic field \mathbf{B} of the site. Ground altitude h_g and geomagnetic field \mathbf{B} are the same as in Section 3.2. Decay, Coulomb scattering, continuous and catastrophic energy loss for muons are implemented, and evaluated at each simulation step. If the muon decays, the propagation is stopped. The energy losses through pair production and photonuclear interactions are taken into account in a continuous way through the Bethe-Bloch formula, while the catastrophic energy loss due to the bremsstrahlung is taken into account in a stochastic way. The calculations are done in a similar manner as in CORSIKA, and presented in great detail in the physics guide [10] of the code.

This procedure was applied successfully with the air shower simulation code AIRES [21] as the primary muon generator, again using QGSJet-II [19] for the high energy interactions. The calculation of the muons at their production point takes about 40 minutes on a Pentium Xeon 2.8 GHz CPU. The calculation of the muon ground distribution at one particular azimuth ϕ then takes only a few minutes on the same machine.

This leads to a total speed up factor of over 1000 with regard to the simulation of the full shower in Section 3.2.

4 Extraction of average muon ground profiles

We have seen in the previous section that it is possible to factorise the ground profile of the muon density n_μ into a normalised density profile p_μ and a global factor N_μ , the total muon number on the ground (see Eq. (2)). The normalised profile p_μ is independent of the primary energy and mass.

In this section, we will parameterise N_μ and p_μ separately for a simulated library of proton showers, and thus will be able to calculate the average ground profile of the muon density n_μ for any combination of energy, zenith, and azimuth angle.

A parameterisation is necessary out of two reasons. Air shower Monte-Carlo codes provide the full particle information on the ground, but only for a discrete choice of (E, θ, ϕ) . Even more, the individual showers contain shower-to-shower fluctuations. The ground profile of muon density in addition has sampling fluctuations, because the density is calculated from a discrete count of particles in a defined sampling area.

The parameterisation of N_μ is straight forward. The parameterisation of p_μ is more complicated and needs two main steps.

In the first step, a linear parameterisation is fitted to the normalised profile of the muon density p_μ^i of each individual raw shower i , that is able to reproduce the functional behaviour inside a single shower. This first fit leads to a set of k parameters $\{a_k\}$ for every shower i .

These parameters show a functional behaviour depending on the direction of the shower:

$$a_k = a_k(\theta, \phi). \quad (8)$$

In the second step, a linear parameterisation in θ and ϕ is fitted to the k -th parameter of every shower, which leads to l coefficients for every parameter a_k .

The result is a $k \times l$ matrix of coefficients, which gives an average, continuous description of $p_\mu(r, \psi; \theta, \phi)$.

The same procedure can be applied to the local muon inclination profile $\theta_\mu(r, \psi; \theta, \phi)$ and to the local muon energy profile $E_\mu(r, \psi; \theta, \phi)$, which also may be important for energy reconstruction from the measured data in a surface array, depending on the specific ground detector³.

³ The effective detection area of a ground detector depends on the muon inclination θ_μ . The amount of ionisation energy loss in a detection material depends (weakly) on the muon energy E_μ .

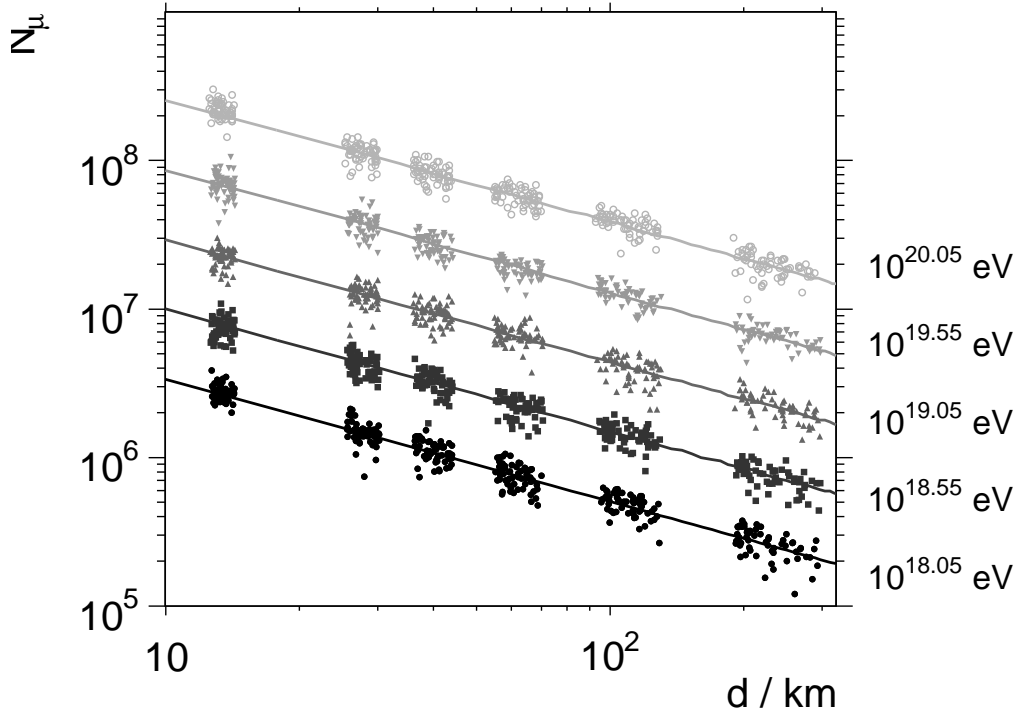


Fig. 6. Simulation of the total muon number on the ground N_μ as function of the distance d between the shower maximum and the ground along the shower axis. Points of different colors are taken from different energy intervals, the average energy in each interval is shown at right side of the plot. The continuous lines are projections of a two-dimensional fit to the simulation (see text).

4.1 Parameterisation of the total number of muons on the ground

The total number of muons on the ground N_μ can be easily extracted from each simulated shower. Since we use proton primaries, N_μ is only a function of zenith angle θ and primary energy E . As discussed in Section 2.3, the E and θ dependence factorise for $\theta > 60^\circ$.

We derive at a very simple functional form, if we plot N_μ not over θ but over $d(\theta)$, the distance between the shower maximum and the point where the shower hits the ground (see Fig. 6). This gives together with Eq. (5) the idea for the empirical formula:

$$\lg N_\mu = C_1 + C_2 \lg(d(\theta)/\text{km}) + \beta \lg(E/10^{18} \text{ eV}), \quad (9)$$

where C_1 , C_2 , and β are constants. For the CORSIKA library, we get:

$$\begin{aligned} C_1 &= 7.3043 \pm 0.0066 \\ C_2 &= -0.8240 \pm 0.0036 \\ \beta &= 0.9352 \pm 0.0020. \end{aligned}$$

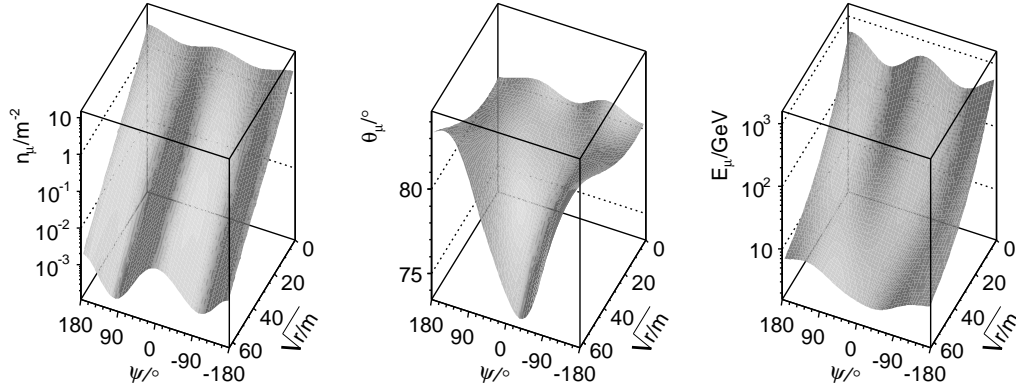


Fig. 7. Average simulated profiles of a) muon particle density, b) muon inclination, and c) muon energy at ground level for $\theta = 80^\circ$ and $\phi = 0^\circ$. The average profiles are derived through a parameterisation from the library in Section 3.2 (see text).

The systematic error of the fit was derived by calculating average residuals as a function of energy, zenith and azimuth angle. It was found to be smaller than 2 %.

4.2 Parameterisation of the normalised muon profile

We will now explain the parameterisation of the normalised profile of muon density p_μ in technical detail. The procedure starts from a library of simulated showers and follows four steps.

A) Coordinate transformation and density calculation. Shower Monte-Carlos deliver muons with ground coordinates. For each shower i , the ground coordinates are projected onto the shower plane coordinate system (see Fig. 1).

On a logarithmic scale, the profile of muon density shows very regular features, if it is plotted in polar coordinates of \sqrt{r} and ψ (compare Fig. 7). The dependency in \sqrt{r} is not far from being linear, therefore \sqrt{r} is an excellent variable for a polynomial expansion.

In these coordinates, we divide the shower plane coordinate system into 30 bins in ψ and 30 bins in \sqrt{r} , ranging from 0 to $\sqrt{4000}$ m.

The raw ground density of muons n_μ^i is derived by counting the number of muons in each cell (including their weight from the thinning), and dividing this number by the area of each cell. In our coordinate system, the corresponding

ground area A_{cell} of each cell is:

$$A_{\text{cell}} = \frac{1}{2 \cos \theta} (\psi_1 - \psi_0) (\sqrt{r_1^4} - \sqrt{r_0^4}), \quad (10)$$

where θ is the zenith angle of the shower.

To normalise the ground profile of muon density $n_{\mu}^i(\sqrt{r}, \psi; \theta_i, \phi_i)$, the density of every cell is further divided by the total number of muons on the ground N_{μ}^i of the shower i . Then, the logarithm of the normalised density is calculated in each cell.

The same projection and binning is applied to parameterise the muon inclination profile $\cos \theta_{\mu}(\sqrt{r}, \psi; \theta_i, \phi_i)$, and the muon energy profile $\lg E_{\mu}(\sqrt{r}, \psi; \theta_i, \phi_i)$.

B) Local parameterisation. The normalised profile $\lg p_{\mu}^i$ of the shower i is now parameterised by a polynomial in \sqrt{r} and a Fourier expansion in ψ .

$$\lg p_{\mu}^i = \sum_{k=0}^3 \hat{r}^k \times \left(\sum_{j=0}^3 a_{kj} \cos(j\psi) + \sum_{j=1}^3 b_{kj} \sin(j\psi) \right) \quad (11)$$

$$\text{with } \hat{r} = 2(\sqrt{r} - \sqrt{r_{\min}})/(\sqrt{r_{\max}} - \sqrt{r_{\min}}) - 1. \quad (12)$$

Here, \hat{r} is the reduced variable of \sqrt{r} that optimises the numerical accuracy of the fit computation. The fit leads to 28 parameters $\{a_{kj}, b_{kj}\}$ per shower. The opposite lobes of μ^+ and μ^- expected from the magnetic deflections are described by the quadrupole term ($j = 2$) of the Fourier expansion. There is also a forward-backward asymmetry described by the dipole ($j = 1$) and octupole terms ($j = 3$).

The choices for the limits of the expansions $k_{\max} = 3$ and $j_{\max} = 3$ are based on comparisons between the raw profiles and the fit. Lower values do not reproduce the main physics with a sufficient accuracy, higher orders would only reproduce statistical fluctuations of the raw profiles at short scales. The raw profiles of the fast simulation contain less fluctuations and can be expanded to higher orders in k and j .

A linear expansion is a key ingredient in our procedure. It allows to use the *linear least squares method* of parameter estimation, which has an exact solution, is unbiased and independent of the distribution of input (see for example [13]).

C) Global parameterisation. Each parameter a_{kj}, b_{kj} of the last step is now regarded as a function of (θ, ϕ) . The parameterisation in ϕ is performed again using the first terms of a Fourier expansion. The parameterisation in θ is done by a polynomial in $d(\theta)$, the distance between the ground and the shower maximum along the shower direction (see Fig. 3). The distance $d(\theta)$ is roughly

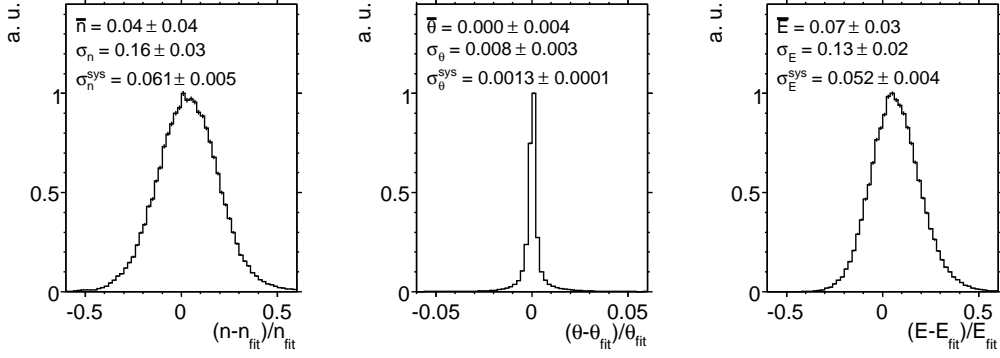


Fig. 8. Residuals of 360 raw profiles versus the parameterisation between $\theta = 60^\circ$ and 88° and $18.0 < \lg E/\text{eV} < 18.1$: a) for the muon density profile, b) the muon inclination profile, and c) the muon energy profile. Mean and r.m.s. of each distribution are given in the plot, as well a systematic error of the parameterisation (see text).

the scale on which the magnetic deflection, divergence and attenuation in a shower grow. It is therefore the ideal variable for the expansion of n_μ .

$$\begin{aligned}
 a_{kj} &= \sum_{m=0}^5 \hat{d}(\theta)^m \left(\sum_{\ell=0}^5 \alpha_{kjm\ell}^a \cos(\ell\phi) + \sum_{\ell=1}^6 \beta_{kjm\ell}^a \sin(\ell\phi) \right) \\
 b_{kj} &= \sum_{m=0}^5 \hat{d}(\theta)^m \left(\sum_{\ell=0}^5 \alpha_{kjm\ell}^b \cos(\ell\phi) + \sum_{\ell=1}^6 \beta_{kjm\ell}^b \sin(\ell\phi) \right) \\
 &\text{with } \hat{d} = 2(d - d_{\min}) / (d_{\max} - d_{\min}) - 1,
 \end{aligned} \tag{13}$$

where \hat{d} is again the reduced variable and

$$\alpha_{kjm\ell}^a, \beta_{kjm\ell}^a, \alpha_{kjm\ell}^b, \beta_{kjm\ell}^b$$

are the final coefficients.

For the parameterisation of $\cos \theta_\mu$ and $\lg E_\mu$, an expansion in $d(\theta)$ is not an ideal choice. Instead, $\hat{d}(\theta)$ in Eq. (13) is replaced by

$$\hat{\theta} = 2(\theta - \theta_{\min}) / (\theta_{\max} - \theta_{\min}) - 1. \tag{14}$$

The three final matrices of $28 \times 66 = 1848$ parameters provide a full description of p_μ , θ_μ and E_μ , which completes our task. An example of the parameterisation is shown in Fig. 7.

4.3 Accuracy of the parameterisation

The parameterisation procedure is applied to 1800 CORSIKA proton showers between $\theta = 60^\circ$ and 88° from the library in Table 1. The raw profiles of the lowest energies $18.0 < \lg E/\text{eV} < 18.1$ are then compared to the parameterisation, because they contain the smallest weights per muon from the thinning (see Section 3.1).

For the analysis, the shower front plane is divided into a 50×50 bin quadratic grid, with a range in x and y of $(-4000 \text{ m}, 4000 \text{ m})$. Only cells are compared, where the raw profile contains more than 100 explicitly tracked Monte-Carlo particles (with varying weights). This cut reduces sampling fluctuations inside the raw profile to an acceptable level.

The result shows Fig. 8. We observe slight shifts of the average residuals, in case of the muon density by 4% and in case of the muon energy by 7%. These shifts are an artifact of our selection, because we compare the parameterisation averaged over all energies with the lowest energy showers. The shifts show the weak energy dependence of the profiles of muon density and muon energy.

The variance σ of the residuals is also given in Fig. 8, it ranges between 1% for the muon inclination profile θ_μ and 16% for the muon density profile n_μ . In the latter case, this is not the true resolution of the parameterisation σ_{param} , as the variance $\sigma(n_\mu)$ also includes shower-to-shower fluctuations $\sigma_{\text{sh-sh}}$ of the raw profile and fluctuations from the density sampling σ_{sampl} :

$$\sigma(n_\mu) = \sqrt{\sigma_{\text{param}}^2(n_\mu) + \sigma_{\text{sh-sh}}^2(n_\mu) + \sigma_{\text{sampl}}^2(n_\mu)}. \quad (15)$$

The size of the last term is difficult to estimate, but was reduced as much as possible by selecting the showers with the lowest weights per particle. The variance σ is therefore an upper limit to σ_{param} .

The shower-to-shower fluctuations of the total muon number N_μ give a large contribution to the variance of muon density profile: $\sigma_{\text{sh-sh}}(n_\mu) = 13\%$ (for proton primaries). These fluctuations only vary the total muon number on the ground N_μ , while the normalised profile p_μ remains constant within 5% (compare Section 2.3). We can subtract the shower-to-shower fluctuations, and obtain

$$\sigma'(n_\mu) = \sqrt{\sigma_{\text{param}}^2(n_\mu) + \sigma_{\text{sampl}}^2(n_\mu)} \approx 10\%. \quad (16)$$

The raw profile of muon density is therefore reproduced by the parameterisation with an accuracy better than 10%.

The parameterisation was further checked against systematic shifts of the average residual as a function of zenith angle θ and azimuth angle ϕ . This

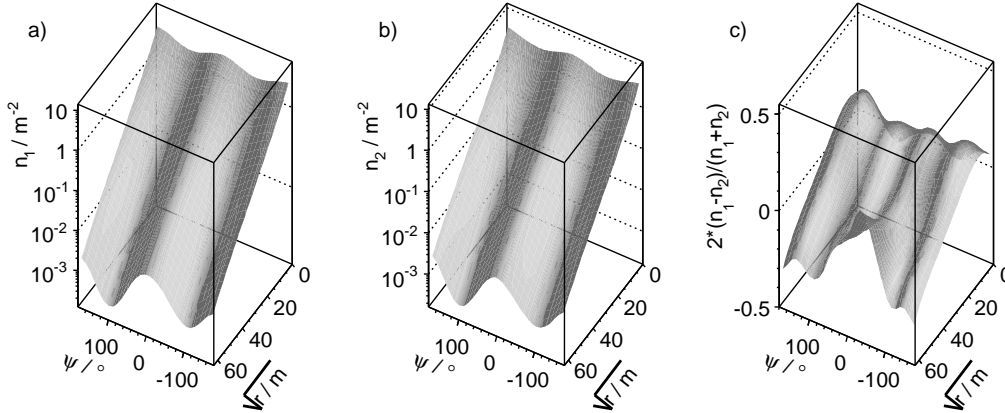


Fig. 9. Average muon density profile on the ground n_μ at $\theta = 80^\circ$, $\phi = 0^\circ$ for a 10^{19} eV proton, derived from a) the full simulation chain (compare Section 3.2), and b) the fast simulation chain (compare Section 3.3). Both simulations use QGSJet-II to model hadronic interactions. The comparison of both is shown in c).

variation σ_{sys} is a systematic uncertainty, and also shown in each profile in Fig. 8. It is smaller than 6 % in any case.

4.4 Comparison of full and fast simulation

We can now do a comparison between the average ground profile of muon density n_μ generated from the full simulation (see Section 3.2), and from the fast simulation (see Section 3.3).

The fast simulation follows the steps in Section 3.3 and uses AIRES [21] together with QGSJet-II [19] as the primary muon generator. For our comparison, 50 proto-showers are generated with AIRES at $\theta = 80^\circ$ with an energy of $E = 10^{19}$ eV. For each shower, 31 azimuth angles in equal distance are calculated with the dedicated muon simulation. The profiles are averaged for every azimuth angle, and parameterised with our method. Because of the special muon unthinning during the fast simulation and the averaging of 50 showers per ground profile, the statistical quality far surpasses that of the full simulation, especially far from the shower axis.

The two parameterisations are then compared, an example for a particular choice of ϕ is shown in Fig. 9. Close to the axis ($r < 2000\text{m}$), the differences in the muon density are within 10 %. Far from the axis ($r > 2000\text{m}$), we find differences up to 40 %. These differences agree quantitatively with a reported systematic differences between CORSIKA and AIRES in the muon density profile far from the shower axis [21].

5 Conclusion and outlook

We have described in this paper a method to extract the average ground profiles of muon density n_μ , muon inclination θ_μ and muon energy E_μ from a library of simulated air showers with zenith angles larger than 60° and ultra-high energies above 10^{18} eV. The parameterisation leads to continuous ground profiles of the mentioned quantities in all relevant variables.

We applied this method to an air shower library of 1800 proton showers simulated with the Monte-Carlo code CORSIKA together with the hadronic interaction models QGSJet-II and FLUKA. We found, that the parameterisation reproduces the raw profiles from the simulation in each point with an accuracy better than 13 %. The systematic bias with respect to different primary energies and shower directions is smaller than 5 %.

We further demonstrated a way to speed up in the detailed Monte-Carlo simulation of the muon component in air showers by a factor of 1000, by discarding the calculation of the electromagnetic component and exploiting an azimuthal symmetry of the muon component at their production point. This is achieved through a small modification of the standard air simulation code AIRES and the use of a dedicated muon propagation code.

A natural application of these ground profiles is in the reconstruction of the primary energy E of an inclined air shower in ground arrays of particle detectors, which sample the local muon density of the shower on the ground. We discussed in detail, how the dependencies of the average profile n_μ can be simplified and exploited in the reconstruction of the primary energy E .

The power of such an energy reconstruction is obvious if only muons contribute to the detected signals. In presence of a non-negligible contribution of the electromagnetic part of the shower to the detected signals (especially in the zenith range $60^\circ \leq \theta \leq 70^\circ$, where the primary electromagnetic component is not fully extinct), dedicated studies are necessary to include the effect from the electromagnetic part into the energy reconstruction.

Acknowledgements

This work was partly funded by the German Federal Ministry for Education and Research BMBF and the German Research Foundation DFG. The computation of the air shower library was supported by a grant of computing time from the Ohio Supercomputer Center. We thank Jim Beatty and the OSC team for making the use of this grant possible.

A part of the air shower simulations and their mass storage were possible through a grant of computing time and storage capability at the Computing Center in Lyon, France, to the Pierre Auger Collaboration. We like to thank the Lyon User Support Team for their support.

For additional support and valuable discussions during the work that led to this paper, we like to thank our colleagues of the Pierre Auger Collaboration.

References

- [1] M. Ave, R. A. Vázquez, and E. Zas, *Astroparticle Physics* **14**, 91 (2000).
- [2] M. Ave *et al.*, *Astroparticle Physics* **14**, 109 (2000), arXiv:astro-ph/0003011.
- [3] M. Ave, J. A. Hinton, R. A. Vázquez, A. A. Watson, and E. Zas, *Phys. Rev. Lett.* **85**, 2244-2247 (2000).
- [4] M. Ave *et al.*, *Phys. Rev. D* **65** (2002) 063007.
- [5] P.Billoir, *Lect. Notes Phys.* **576** (2001), and references therein.
- [6] L. Cazón, R. A. Vázquez, A. A. Watson, and E. Zas, *Astropart.Phys* **21**, 71-86 (2004).
- [7] A. Fassó, A. Ferrari, J. Ranft, and P. Sala, CERN-2005-10 (2005), INFN/TC 05/11, SLAC-R-773, 2005.
- [8] R.S. Fletcher, T.K. Gaisser, P. Lipari, and T. Stanev, *Phys. Rev. D* **50** (1994) 5710; J. Engel, T.K. Gaisser, P. Lipari, and T. Stanev, *Phys. Rev. D* **46** (1992) 5013; R. Engel, T.K. Gaisser, T. Stanev, *Proc. 26th Int. Cosmic Ray Conf.*, Salt Lake City (USA), **1** (1999) 415
- [9] T. Gaisser, *Cosmic Rays and Particle Physics*, Cambridge University Press (1990).
- [10] D. Heck *et al.*, Report FZKA 6019, Karlsruhe (1998).
- [11] A. M. Hillas, *Nucl. Phys. B (Proc. Suppl.)* **52B**, 29 (1997).
- [12] D. Heck and J. Knapp, Report FZKA 6097B, Karlsruhe (1998).
- [13] F. James, *Statistical Methods in Experimental Physics*, 2nd Edition, World Scientific Publishing (2006).
- [14] N. N. Kalmykov and S. Ostapchenko, *yad. Fiz.* **56** (1993) 105; *Phys. At. Nucl.* **56** N3 (1993) 346; N.N. Kalmykov, S.S. Ostapchenko and A.I. Pavlov, *Izv. RAN Ser. Fiz.* **58** (1994) N12 p.21; N.N. Kalmykov, S.S. Ostapchenko and A.I. Pavlov, *Bull. Russ. Acad. Science (Physics)* **58** (1994) 1966; N.N. Kalmykov, S.S. Ostapchenko and A.I. Pavlov, *Nucl. Phys. B (Proc. Suppl.)* **52B** (1997) 17.

- [15] B. Keilhauer *et al.*, *Astroparticle Physics* **22**, 249 (2004).
- [16] M. Kobal, Internal note of the Pierre Auger Observatory GAP-2000-061 (2000).
- [17] J. Matthews, *Astroparticle Physics* **22**, 387 (2005).
- [18] National Geophysical Data Center (2007), <http://www.ngdc.noaa.gov/seg/geomag/geomag.shtml>.
- [19] S. Ostapchenko, *Proc. of the ISVHECRI* (NESTOR Institute, Pylos, Greece, 2006), Vol. 151, p. 143 and 147, arXiv: hep-ph/0412332 (2004) and hep-ph/0501093 (2005).
- [20] The Pierre Auger Collaboration, *Science* **318**, 938 (2007).
- [21] S. J. Sciutto, *Proc. of the 27th ICRC*, Copernicus Gesellschaft, Hamburg, Germany, (2001), arXiv:astro-ph/0106044v1.
- [22] M. Unger for the Pierre Auger Collaboration, *Proc. of the 30th ICRC* (2007).
- [23] K. Werner, F.-M. Liu, and T. Pierog, *Physical Review C (Nuclear Physics)* **74**, 11 (2006), <http://link.aps.org/abstract/PRC/v74/e044902>.
- [24] K. Werner and T. Pierog, *AIP Conf. Proc.* **928**, 111 (2007).
- [25] W.-M. Yao et al. (Particle Data Group), *Journal of Physics G: Nuclear and Particle Physics* **33**, 1 (2006), and 2007 partial update for the 2008 edition.

A The CORSIKA library: Thinning and energy thresholds

For the correct simulation of inclined showers, CORSIKA [10] is compiled with the CURVED and UPWARD options. The SLANT option would have been useful as well, but was not ready at the time of the simulation.

For the thinning parameters, a so called “optimal thinning” strategy is used [12, 16]. In this strategy, the energy at which the thinning starts E_{thin} is a function of the primary energy E , as well as the allowed maximum weight w_{max} for a single Monte-Carlo particle:

$$\begin{aligned}
 E_{\text{thin}} &= 10^{-6} E \\
 w_{\text{max}}^{\text{had},\mu} &= 10^{-6} E/\text{GeV} \\
 w_{\text{max}}^{\text{e},\gamma} &= 10^{-4} E/\text{GeV} \quad .
 \end{aligned}
 \tag{A.1}$$

As a quality trade-off, a lower maximum weight for hadrons and muons $w_{\text{max}}^{\text{had},\mu}$ is chosen than for electrons and photons $w_{\text{max}}^{\text{e},\gamma}$, since muons dominate in inclined showers. An energy dependent $w_{\text{max}}(E)$ makes sure, that the amount of actually calculated particles remains roughly the same, which is directly proportional to the calculation time.

Muons and hadrons are followed in the simulation down to energies of $E_{\text{thres}}^{\text{had},\mu} = 0.1 \text{ GeV}$, electrons (positrons) and photons down to $E_{\text{thres}}^{e,\gamma} = 250 \text{ keV}$.

B Thinning and energy thresholds of the Fast Simulation

To generate the muon distribution at their production point for the fast simulation explained in Section 3.3, the following thinning and energy thresholds are used in the air shower code AIRES [21]:

$$\begin{aligned}
 \text{Thinning} &= 5 \cdot 10^{-7} \\
 \text{ThinningWF} &= 1 \\
 E_{\text{thres}}^{\gamma} &= 200 \text{ MeV} \\
 E_{\text{thres}}^e &= 400 \text{ MeV} \\
 E_{\text{thres}}^{\mu} &= 100 \text{ MeV} \\
 E_{\text{thres}}^{\text{meson}} &= 150 \text{ MeV} \\
 E_{\text{thres}}^{\text{nucleon}} &= 125 \text{ MeV} \quad .
 \end{aligned}
 \tag{B.1}$$

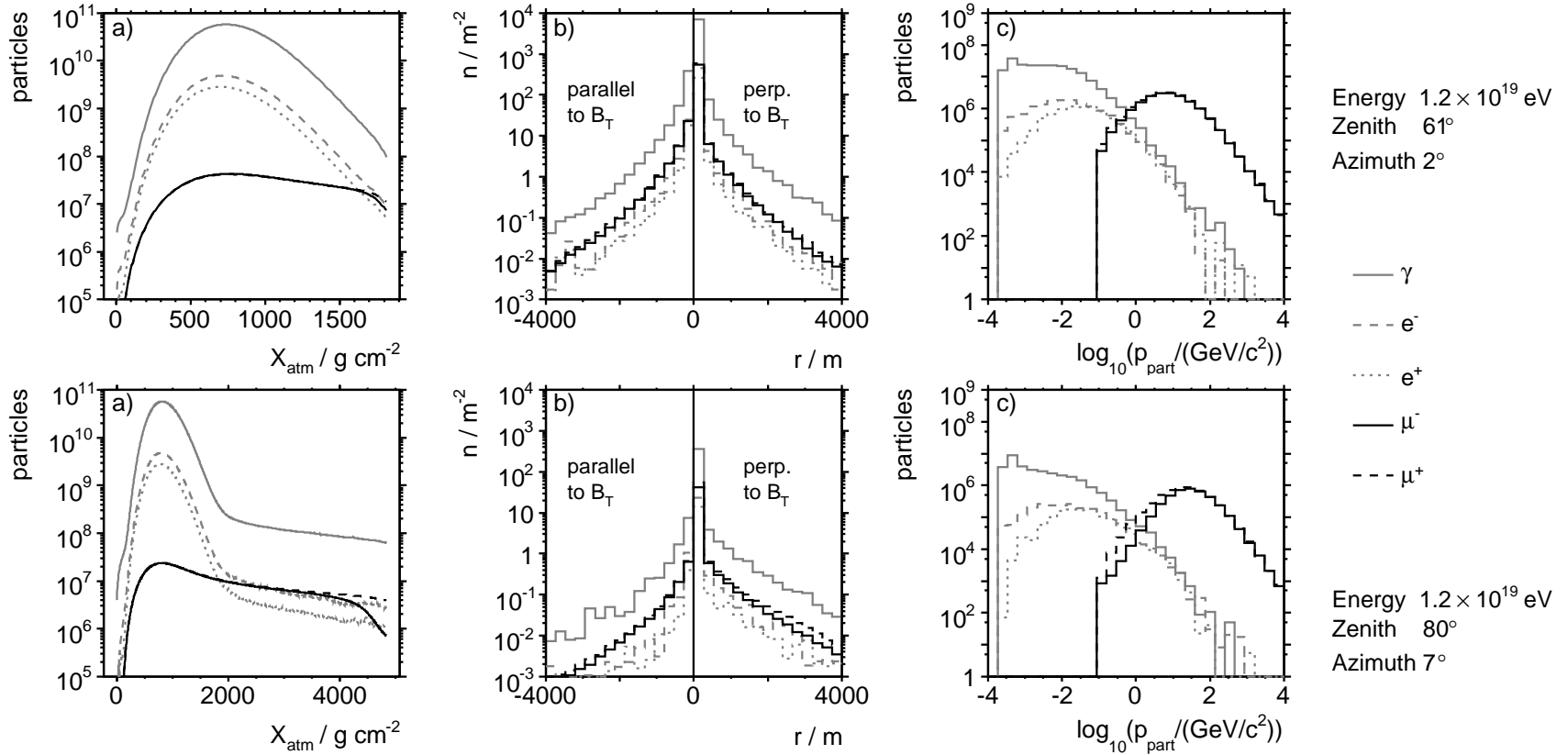


Fig. B.1. Comparison of two inclined proton showers, simulated with CORSIKA/EPOS/FLUKA [7, 10, 23]. From left to right: a) total particle number vs. passed atmospheric depth, b) particle number per tank on the ground vs. radial distance from the shower axis, c) energy distribution on the ground. In b), $r > 0$ relates to particles collected within $\pm 10^\circ$ around the direction perpendicular to the projected geomagnetic field \mathbf{B}_T and $r < 0$ relates to particles collected within $\pm 10^\circ$ around the direction parallel to \mathbf{B}_T (see Section 2.1). In all plots, only particles above certain energy thresholds are shown: $E_{\text{thres}} = 250 \text{ keV}$ for electromagnetic particles and $E_{\text{thres}} = 0.1 \text{ GeV}$ for everything else. The low energy photon peak in c) is caused by e^+/e^- annihilation. The particle depletion along \mathbf{B}_T in b) for $\theta = 80^\circ$ is the result of geomagnetic deflection.